Chemical Engineering Journal 146 (2009) 439–448

Contents lists available at ScienceDirect

Chemical Engineering Journal

journal homepage: www.elsevier.com/locate/cej

Parametric study on mixing of two fluids in a three-dimensional serpentine microchannel

Mubashshir Ahmad Ansari, Kwang-Yong kim*

Department of Mechanical Engineering, Inha University, 253 Yonghyun-Dong, Nam-Gu, Incheon 402-751, Republic of Korea

ARTICLE INFO

Article history:
Received 28 June 2008
Received in revised form
28 September 2008
Accepted 8 October 2008

Keywords:
Mixing
Numerical analysis
Diffusion
Laminar flow
Three-dimensional serpentine microchannel
Parametric study

ABSTRACT

A flow analysis method using Navier–Stokes equations has been applied to a parametric investigation of mixing two fluids in a three-dimensional serpentine microchannel, which has not been reported so far. The serpentine microchannel with "L-shaped" repeating units is found to be effective in mixing fluids at Reynolds numbers, 1, 10, 35 and 70. Mixing performance and pressure drop characteristics with two geometrical parameters, i.e., the ratio of channel height to channel width and the ratio of the length of a straight channel in an "L-shaped" unit to the channel width, have been analyzed at four different Reynolds numbers. A mixing index has been used to quantify and elucidate mixing behavior in the microchannel. The vortical structure of the flow in the channel is also analyzed to identify the relationship with mixing performance. The results reveal that mixing and pressure drop characteristics in a serpentine channel are very sensitive to the geometric parameters, showing different behavior at various Reynolds numbers.

1. Introduction

Mixing of liquids in microfluidic devices presents a considerable challenge as the flow is predominantly laminar. In the past decade, there has been remarkable achievement in both academic and industrial realms in the development of micromixers. A number of active and passive micromixers working on different operating principles have been reported in the literature [1,2]. Active micromixers use an external source of energy, and are difficult to fabricate. However, passive micromixers are easy to fabricate and integrate with other microdevices and they operate without external energy. A three-dimensional serpentine micromixer, a kind of passive micromixer, has been reported to be very effective in mixing at low Reynolds numbers. The geometry design is aimed at enhancing the mixing of fluids by implementing chaotic advection. A two-dimensional serpentine micromixer meanwhile integrates a square-wave type channel. These geometries have been studied in relation to mixing analyses by many researchers.

Liu et al. [3] experimentally investigated the mixing performance of a three-dimensional serpentine micromixer with "C-shape" repeating units for Reynolds numbers from 6 to 70. The results were compared with square-wave and simple smooth channels for various Reynolds numbers. It has been reported that the mixing capability of a channel increases with an increase in Reynolds number [3,4]. Beebe et al. [4] qualitatively analyzed the mixing performance of a three-dimensional serpentine microchannel by both experiment and numerical investigations for a range of Reynolds number from 1 to 20. The geometry was a "L-shape" repeating unit with channel dimensions of 300 μm × 300 μm. They also suggested that the mixing increases with an increase in the Reynolds number. Lin and Yang [5] numerically studied chaotic mixing of two fluids in a planar serpentine mini-channel by introducing alternating convergent–divergent cross-sections for a Reynolds number of 160. They analyzed the three-dimensional flow field and distribution of concentration. The result reveals improved mixing performance due to enhanced stretching and folding of the fluid interfaces. Yang and Lin [6] experimentally and numerically analyzed the mixing and separation of two fluids in a planar serpentine micromixer. They analyzed the effect of density difference of the fluid on the mixing performance of the channel, and suggested that fluids can be mixed effectively by using a curved channel or other complicated channels at high speed. Liu et al. [7] conducted a numerical study on mixing of two miscible fluids for planar and three-dimensional serpentine micromixers. The effects of the fluid properties (e.g., viscosity, density and diffusivity) and large concentration gradient on the mixing behavior were investigated in these microchannels for a range of Reynolds number from 1 to 10.

* Corresponding author. Tel.: +82 32 872 3096; fax: +82 32 868 1716.
E-mail address: kykim@inha.ac.kr (K.-Y. kim).

1385-8947/$ – see front matter © 2008 Elsevier B.V. All rights reserved.
doi:10.1016/j.cej.2008.10.006

Nomenclature

A	area (m^2)
c	mass fraction
d	length of channel-d (m)
D	diffusivity of the fluid ($m^2\ s^{-1}$)
F	objective function
h	channel height (m)
L_o, L_c, L_e	lengths of channel (m)
M	mixing index
n	number of "L-shaped" repeating unit
N	number of sampling points
P, Δp	pressure and pressure drop in channel (Pa)
Pi	Pitch of "L-shaped" repeating unit
Re	Reynolds number
s	coordinate of channel-d
v_x, v_y, v_z	components of velocity in x-, y- and z-direction ($m\ s^{-1}$)
w	channel width (m)
x, y, z	streamwise, spanwise, and cross-streamwise coordinates

Greek letters

μ	absolute viscosity of fluid ($kg\ m^{-1}\ s^{-1}$)
ρ	fluid density ($kg\ m^{-3}$)
σ	variance
ω	vorticity (s^{-1})
Ω	circulation ($m^2\ s^{-1}$)

Kang et al. [8] studied mixing behavior in a planar serpentine channel with and without external actuation of rigid particles. They reported that the efficiency of the mixing process can be increased by applying a periodic external force on a single rigid particle, thereby changing the trajectory of the particle. The mixing of a fluid is also dependent on the strength of the external force. Lee et al. [9] fabricated and analyzed a three-dimensional serpentine channel with a round bottom for mixing fluids in a range of Reynolds number from 10 to 90. The bottom was modified to a round shape with the aim of preventing clogging and loss of the sample at the corners of the channel. The study, however, did not report on the effect on mixing as compared to a flat bottom. Chen and Cho [10] analyzed mixing characteristics for an electrokinetically driven flow through microchannels with a wavy surface. The wavy shape increases the mixing performance by increasing the interfacial contact area between two fluid streams in comparison with a simple straight microchannel.

Table 1
Properties of fluids at 20 °C.

Fluid	Density ($kg\ m^{-3}$)	Viscosity ($kg\ m^{-1}\ s^{-1}$)	Diffusivity ($m^2\ s^{-1}$)
Water	9.998×10^2	0.9×10^{-3}	1.2×10^{-9}
Ethanol	7.890×10^2	1.2×10^{-3}	1.2×10^{-9}

It is clear that a serpentine geometry is effective in enhancing the mixing of fluids by creating transverse flow structures. However, there have been no reports in the literature on a systematic investigation of the effects of geometric parameters on mixing performance and fluid flow characteristics of three-dimensional serpentine channels.

In the present work, numerical analysis of mixing in a three-dimensional serpentine channel have been performed to investigate mixing behavior and fluid flow characteristics with geometric parameters as well as Reynolds number. Mixing in the channel has been analyzed by using Navier–Stokes equations with two working fluids, water and ethanol. Pressure drop characteristics have also been analyzed. Effects of two design parameters of a three-dimensional serpentine microchannel on the mixing behavior have been found for four Reynolds numbers, from 1 to 70.

2. Physical model and numerical analysis

Fig. 1 shows a schematic model of the three-dimensional serpentine microchannel with repeating "L-shape" units. Two different fluids enter from two inlets, as shown in the figure, and there is an outlet on the right side. Water and ethanol have been selected as the two working fluids for mixing. The properties of the fluids are given in Table 1. The main serpentine channel is joined to the inlets at a T-joint. The width of the channel, w, is kept constant for all repeating "L-shape" units and the remaining part of the main channel at 300 μm, while the width of the inlet channels is half that of the main channel. The length of the straight part of the main channel near inlet, L_o, has been fixed as 900 μm while the other portions of the channel lengths, L_c and L_e, vary with the value of d/w and number of "L-shape" units. However, the total length of the main channel is fixed as 12.9 mm, which is the sum of the channel section lengths, i.e. L_o, L_c, and L_e. The length, L_c, can be expressed as nPi, where n is the number of units and Pi (equal to $(w + d)$) is the pitch of the "L-shape" repeating units. The number of "L-shape" repeating units for $d/w = 0.03$, 0.5, 1.0 is 34, 24, 18 and 14, respectively. The analysis has been performed for Reynolds numbers ranging from 1 to 70. The Reynolds number is evaluated under the assumption that both working fluids are water.

Two geometric parameters, i.e., h/w and d/w, shown in Fig. 1, vary from 0.5 to 1.5 and from 0.03 to 1.5, respectively. Although previous works [3,4] performed analyses for two different values

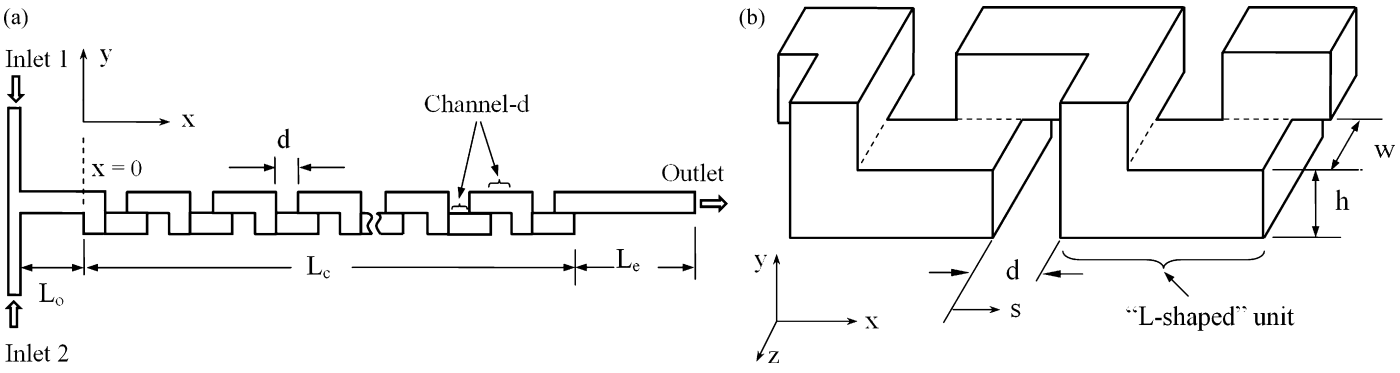

Fig. 1. Geometry of three-dimensional serpentine channel.

of h/w, 1.0 and 0.5, the effect of this parameter on the mixing performance has not been reported.

Numerical analyses of flows in the three-dimensional serpentine channel have been performed using the commercial code ANSYS CFX-10.0 [11], a general purpose code that solves Navier–stokes equations using the finite volume method via a coupled solver. The steady continuity and momentum (Navier–Stokes) equations solved in this work are represented as follows:

$$\nabla \cdot \vec{V} = 0 \tag{1}$$

$$\rho(\vec{V} \cdot \nabla)\vec{V} = \nabla p + \mu \nabla^2 \vec{V} \tag{2}$$

A high quality mesh is critical to achieve accurate results, especially for mixing analyses. ANSYS ICEM 10.0 was used to make a hexahedral grid for the full model. Structured meshing provides the advantage of better control in completely packing all the corners with a sufficient number of nodes as compared to unstructured meshing for analyzing the effect of geometry on mixing.

The numerical simulation is not free from numerical diffusion error, which arises from the discretization of the convection terms in the Navier–Stokes equation. In the present case, the advection terms have been discretized by using a bounded second-order differencing scheme, which is an upwind scheme with a second-order correction [11]. While the numerical diffusion cannot be completely ignored, it can be minimized by adopting certain techniques [12].

The boundary conditions for the model have been set as the normal velocity at the two inlets and zero static pressure at the outlet. The two fluids are brought into contact and start to mix in the T-joint prior to entering the main serpentine channel with repeating "L-units". The wall has been assigned no slip conditions. The properties of the water and ethanol have been taken at 20 °C, and are listed in Table 1. The diffusivity for both water and ethanol is 1.2×10^{-9} m^2 s^{-1}. The solutions are considered to have attained convergence for a rms residual value of 10^{-6}.

The variance of species is determined in a cross-section of the mixing channel perpendicular to the main flow. The variance is based on the concept of the intensity of segregation, which is based on the variance of the concentration with the mean concentration. To evaluate the degree of mixing in the micromixer, the variance of the mass fraction of the mixture in a cross-section normal to the flow direction is defined as

$$\sigma = \sqrt{\frac{1}{N}\sum (c_i - \bar{c}_m)^2} \tag{3}$$

where N is the number of sampling points inside the cross-section, c_i is the mass fraction at sampling point i, and $\bar{c}_m$ is the optimal mixing mass fraction. In this work, N on each plane was more than 400 in order to ensure high accuracy, and the sampling points are equidistant on the cross-sectional plane. The values at the sampling points are obtained by interpolations with the values at adjacent computational grids. The mixing index at an axial location is defined so as to evaluate the degree of mixing of the fluids on a plane perpendicular to the flow direction as follows:

$$M = 1 - \sqrt{\frac{\sigma^2}{\sigma_{\max}^2}} \tag{4}$$

where $\sigma_{\max}$ is the maximum variance over the data range. The variance is maximal for completely unmixed fluids and minimal for completely mixed fluids. The actual path of the flow along the streamline in the channel will be longer than the distance taken in x-direction. However, for simplicity in the analysis, the values have been calculated along the x-direction instead of along streamlines.

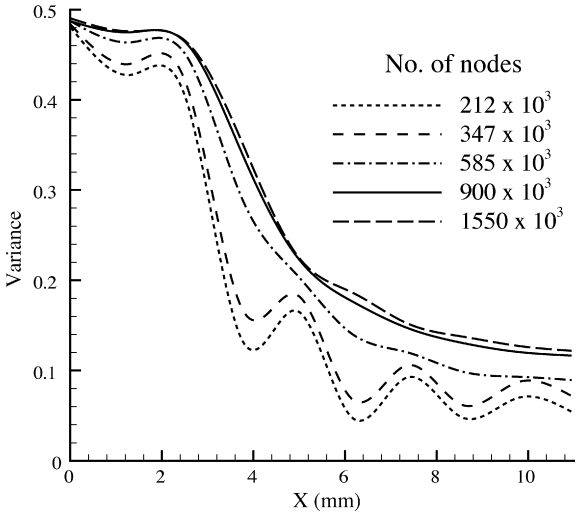

Fig. 2. Grid independency test.

3. Results and discussion

A grid dependency test has been carried out to find the optimal number of grids and to ensure that the solution is independent of the grid size. Six different structured grid systems with the number of grids ranging from 212×10^3 to 1550×10^3 were tested, as shown in Fig. 2. The distribution of the variance of the mass fraction along the serpentine channel was evaluated with an increasing number of grids. The grid distribution was checked and adjusted in each case due to the complicated geometry of the channel. The density of the grid was maintained higher at bend regions in order to capture the flow structure precisely in the region where the flow changes rapidly. Finally, from the results of the grid dependency test, 900×10^3 was selected as the optimum number of grids. An example of the structured grid system employed in this work is shown in Fig. 3.

The present parametric study has been performed for a three-dimensional serpentine channel with "L-shape" repeating units with w/h and d/w as the two design parameters. The mixing index has been selected as a parameter to quantify the mixing performance of the microchannel. The analysis has been carried out for a range of Reynolds number from 1 to 70.

Fig. 4 presents a comparison of the present numerical results with previous experimental and numerical results obtained by Beebe et al. [4], shown in Fig. 4(a) and (b), respectively. The mass fraction distribution of ethanol on a plane drawn at the middle of the channel has been plotted. The previous numerical result [4] does not provide information about the exact location of the plot. The experimental result is an image of the flow captured by a CCD camera for the whole channel depth while the present compu-

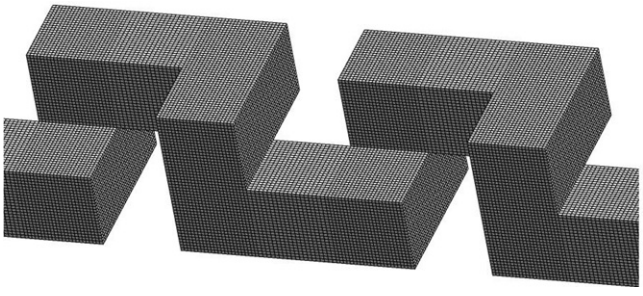

Fig. 3. Example of structured grid system ($h/w = 1.0$ and $d/w = 1.0$).

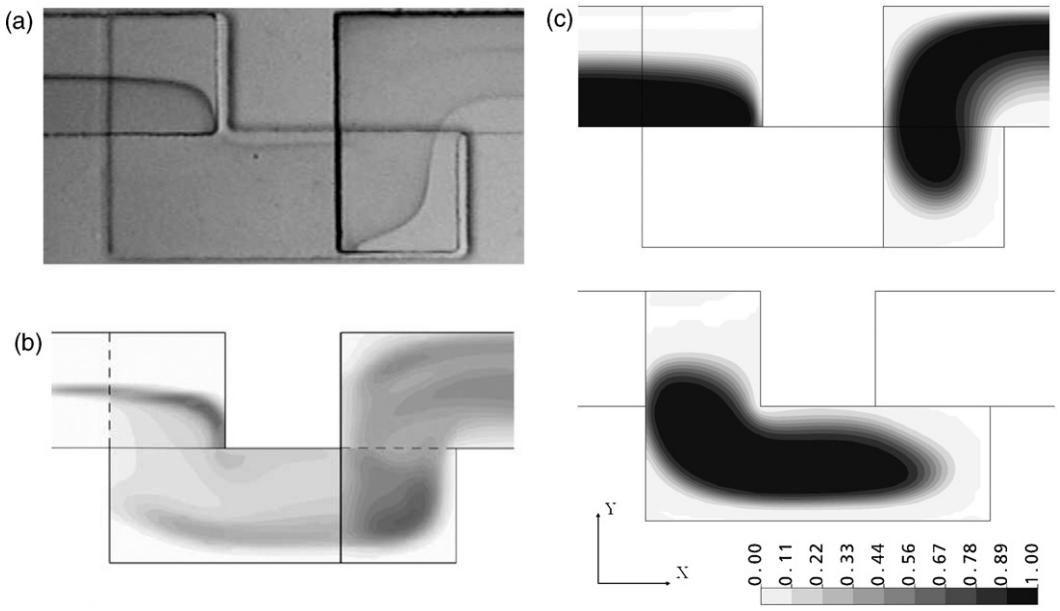

Fig. 4. Comparison with previous results; (a) experimental result, (b) previous numerical result (Beebe et al. [4]), and (c) present numerical result, for mass fraction distribution of ethanol in 3rd L-shaped unit at $Re = 10$.

tational image shown in Fig. 4(c) is captured on a specific plane. However, qualitatively, the image obtained in the present analysis corresponds well with previous experimental and numerical results. Since there is no available quantitative experimental data for a serpentine micromixer, it was not possible to validate the numerical results in more detail.

Fig. 5 shows mass fraction distributions of ethanol on *yz*-plane perpendicular to the main flow direction for three grid systems with the number of nodes, 347×10^3, 900×10^3 and 1550×10^3, respectively, at two axial locations, $x = 1.65$ and 2.25 mm. The plane is drawn at the turn between two "L-shaped" repeating units where fluid undergoes a turning flow. The first axial position is located between second and third "L-shaped" repeating units, and the second axial position between fourth and fifth units. The two axial positions have been selected due to the presence of long stretched interface of the two fluids to clearly compare the mass fraction as a function of number of nodes. The numerical solution of Navier–stokes equation has numerical errors introduced due to discretization of the convective terms. Qualitative comparison of the mass fraction shows wider interface of the fluids for the coarse grid system with the number of nodes 347×10^3 compared to the other two fine grid systems. Hence, the grid system with smaller number of nodes (i.e. larger grid distances) shows higher mixing due to numerical diffusion which is also depicted in Fig. 2. As the number of nodes is increasing, the width of interface of the fluid is becoming thinner. Hence, it becomes obvious that the numer-

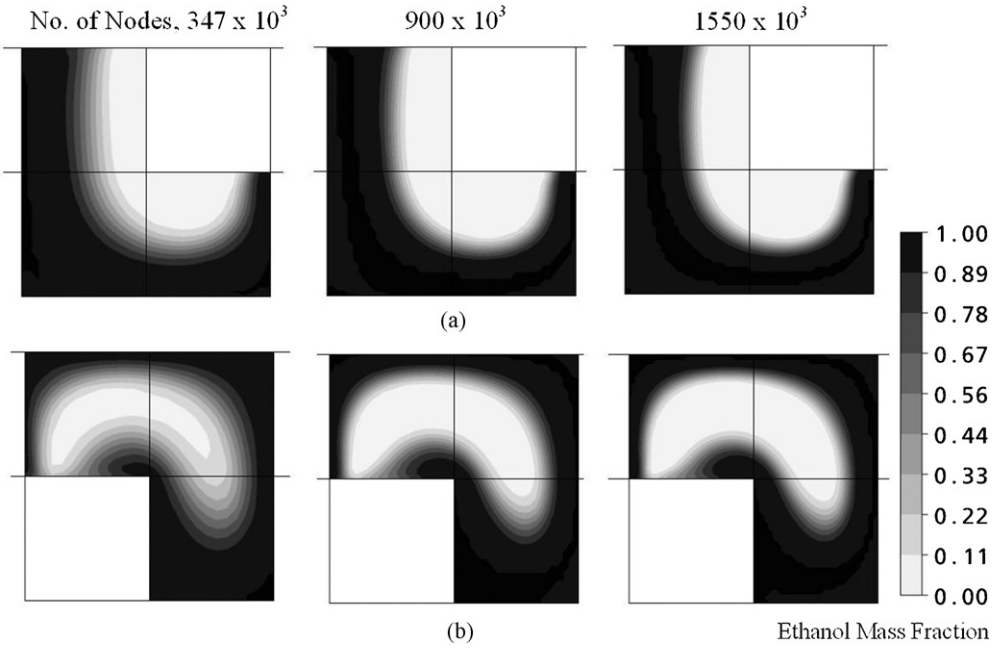

Fig. 5. Mass fraction distribution of ethanol vs. number of nodes for $Re = 10$, $d/w = 1.0$, at axial distances, (a) $x = 1.65$ mm and (b) $x = 2.25$ mm.

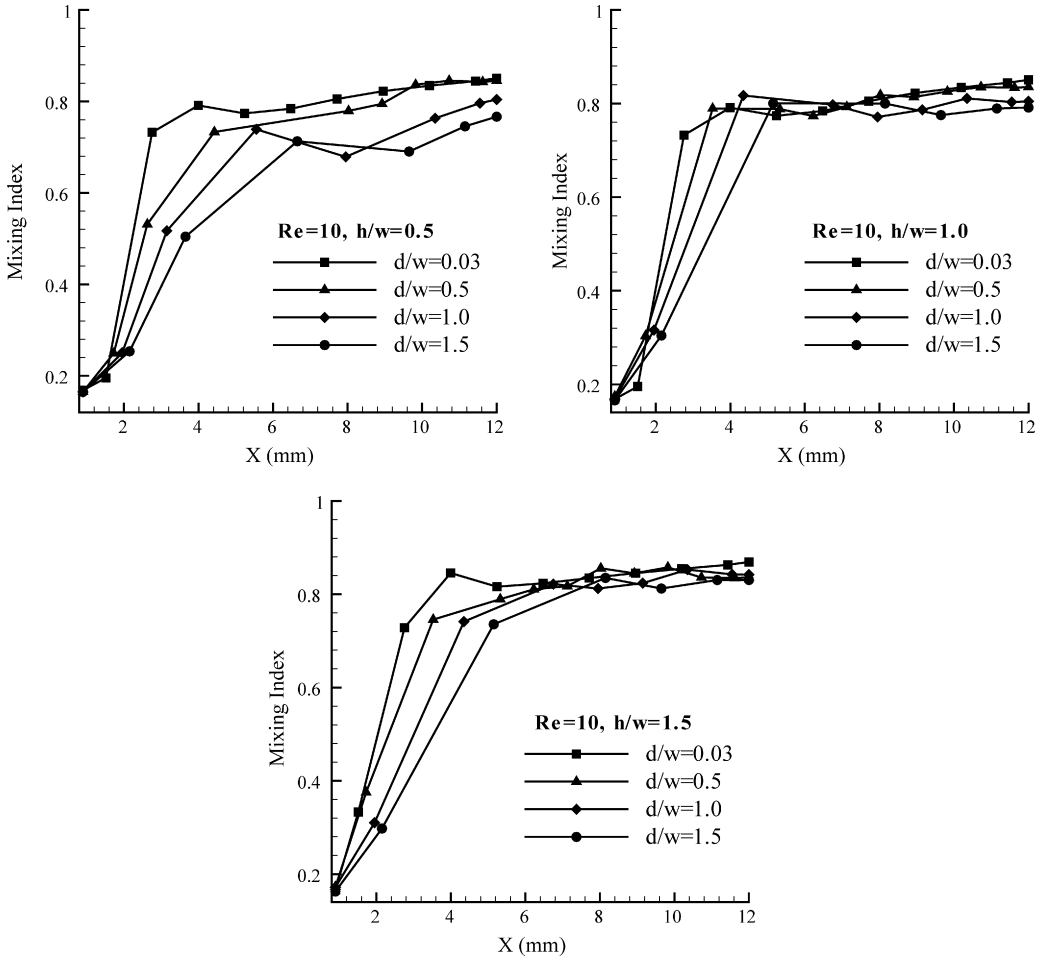

Fig. 6. Effects of d/w on mixing at $Re = 10$; (a) $h/w = 0.5$, (b) $h/w = 1.0$, and (c) $h/w = 1.5$.

ical solutions predict higher value of the mixing than the actual mixing taking place. The presence of numerical diffusion in the solutions cannot be completely eliminated, but can be reduced by adopting certain techniques. Hardt and Schonfeld [12] reported that numerical diffusion can be minimized by selecting the edges of grid cells parallel to local flow velocity. This condition is difficult to be attained in the serpentine channel near bends where flow field is complex. Instead, higher density of the grid can be selected to reduce numerical diffusion.

Fig. 6 shows the effect of the geometric parameter d/w on the mixing performance of the serpentine microchannel. Mixing indexes are plotted along the channel length in the x-direction for four values of d/w, 0.03, 0.5, 1.0, and 1.5, as well as for three values of h/w, 0.5, 1.5, and 1.5 at a Reynolds number of 10. The curve is plotted by evaluating the value of the mixing index on yz-planes drawn in the middle section of alternate channel-d. Channel-d is the straight section of the "L-shape" unit, as indicated in Fig. 1(a). This figure shows that the two fluids are mixed rapidly in the initial part of the channel. Beyond a certain length of the serpentine channel, the mixing index becomes relatively constant. The mixing performance of the channel generally improves with a decrease in the value of d/w. Furthermore, the gradient of the mixing index in the initial part of the channel increases as d/w decreases.

Fig. 7 shows vector plots on yz-planes in channel-d at $Re = 10$ and $h/w = 1.0$. In the initial region of the channel ($s/d = 0.16$ and 0.33), the flow is visualized with the presence of a strong transverse flow structure along with a single vortex near the bottom of the channel wall. However, as the flow passes through the channel, the vortex disappears beyond $s/d = 0.33$, and the strength of the transverse flow reaches a minimum around the middle of the channel-d ($s/d = 0.50$). The strength of the transverse flow then increases again, as the flow turns through the bend of "L-shape" unit. The flow field is influenced by the presence of the bend at the end of channel-d.

Fig. 8 shows the vector plots at $Re = 1$. At this low Reynolds number, the vortical motion disappears and the transverse flow becomes simpler. The flow only changes direction by 90° from the inlet to the outlet of channel-d. As shown in these figures, the complexity of the flow in channel-d is a function of the Reynolds number.

Development of normalized streamwise vorticity on the yz-plane along channel-d of a "L-shape" unit at $Re = 10$, $h/w = 1.0$, and $d/w = 1.5$ is presented as contour plots in Fig. 9 for the third L-shape unit. The following equation shows the expression for vorticity; ω_x is the x-direction component and v_z and v_y are the components of velocity in the z- and y-directions, respectively.

$$\omega_x = \left(\frac{\partial v_z}{\partial y} - \frac{\partial v_y}{\partial z} \right) \tag{5}$$

Two clearly distinguishable regions of peak intensity with opposite signs exist inside the initial region of the channel. However, as the flow proceeds, peak intensity regions around the center of the channel disappear, and the peak values are found near the centers of the side walls. The level of peak vorticity decreases

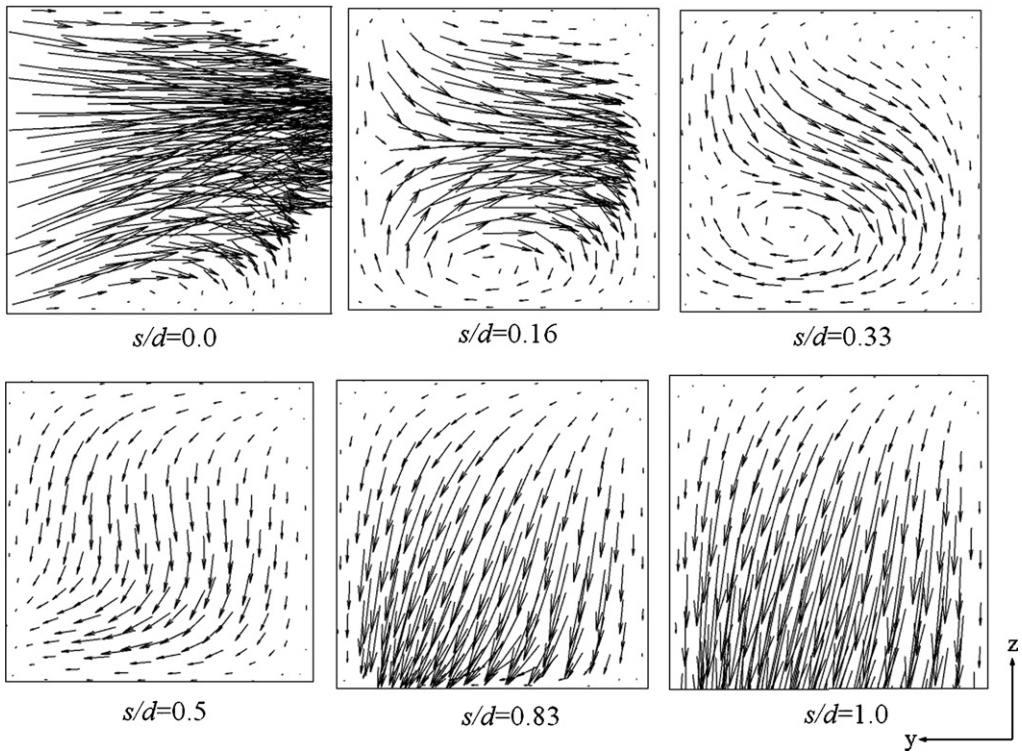

Fig. 7. Vector plots on *yz*-planes in channel-d ($Re = 10$, $h/w = 1.0$, and $d/w = 1.0$).

rapidly near the inlet, remains low in the relatively long section along the channel, and rapidly increases again near the exit. The intensity of the vorticity is expected to be related to the mixing of fluids.

Fig. 10 shows the plot of normalized circulation on the *yz*-plane with a semi-log scale along channel-d for $h/w = 1.0$ and $d/w = 1.5$ at Reynolds numbers of 1, 10, 35, and 70. The circulation on the *yz*-plane, Ω_x is calculated by integrating the streamwise vorticity over the entire area of the *yz*-plane of the channel as follows:

$$\Omega_x = \int_{A_{yz\text{-plane}}} \left(\frac{\partial v_z}{\partial y} - \frac{\partial v_y}{\partial z} \right) \mathrm{d}y\, \mathrm{d}z \tag{6}$$

The circulation is highest at the inlet ($s/d = 0.0$) of the channel-d at all Reynolds numbers, and decreases rapidly within a short distance of $s/d = 0.1$. On the other hand, near the exit ($s/d = 0.9$–1.0) of channel-d, the circulation increases rapidly. The turning flow through the 90° bend at the inlet and exit of the channel-d likely accounts for achieving the highest values at the inlet and the exit of the channel-d. The strength of circulation increases with an increase in the Reynolds number throughout most of channel-d. For all four Reynolds numbers, except in the regions defined by 10% of the channel length near the inlet and exit, respectively, the circulation shows relatively uniform values. The rate of the decrease in the value of circulation near the inlet to channel-d depends strongly on the Reynolds number. The rate decreases rapidly as the Reynolds number increases. The vorticity induced at higher Reynolds numbers with stronger inertia force is able to sustain the friction force, and hence a lower drop in the value of circulation is observed near the inlet.

Fig. 11 shows the effects of d/w on the circulation distribution in channel-d at $Re = 1$. Higher circulation is observed throughout most of channel-d at lower channel lengths. At the minimum length of channel-d at $d/w = 0.03$, the circulation is almost constant throughout the channel. However, near the inlet and exit of the channel, the circulation for the other values of d/w becomes

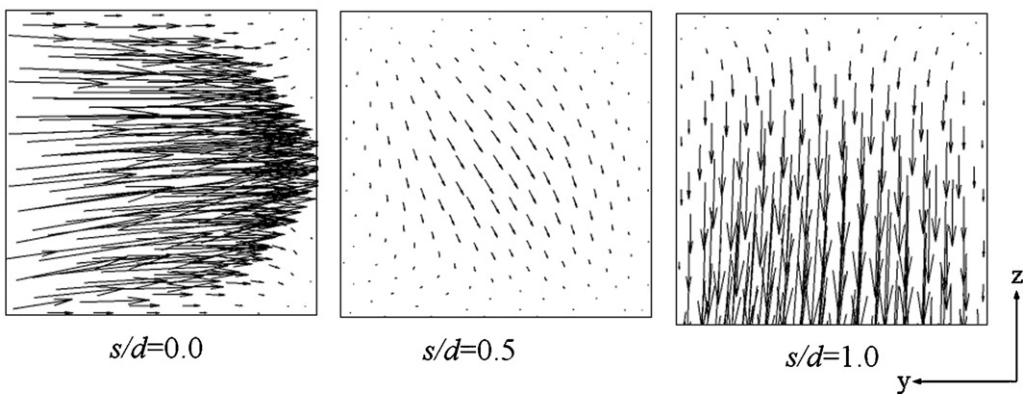

Fig. 8. Vector plots on *yz*-planes in channel-d ($Re = 1$, $h/w = 1.0$, and $d/w = 1.0$).

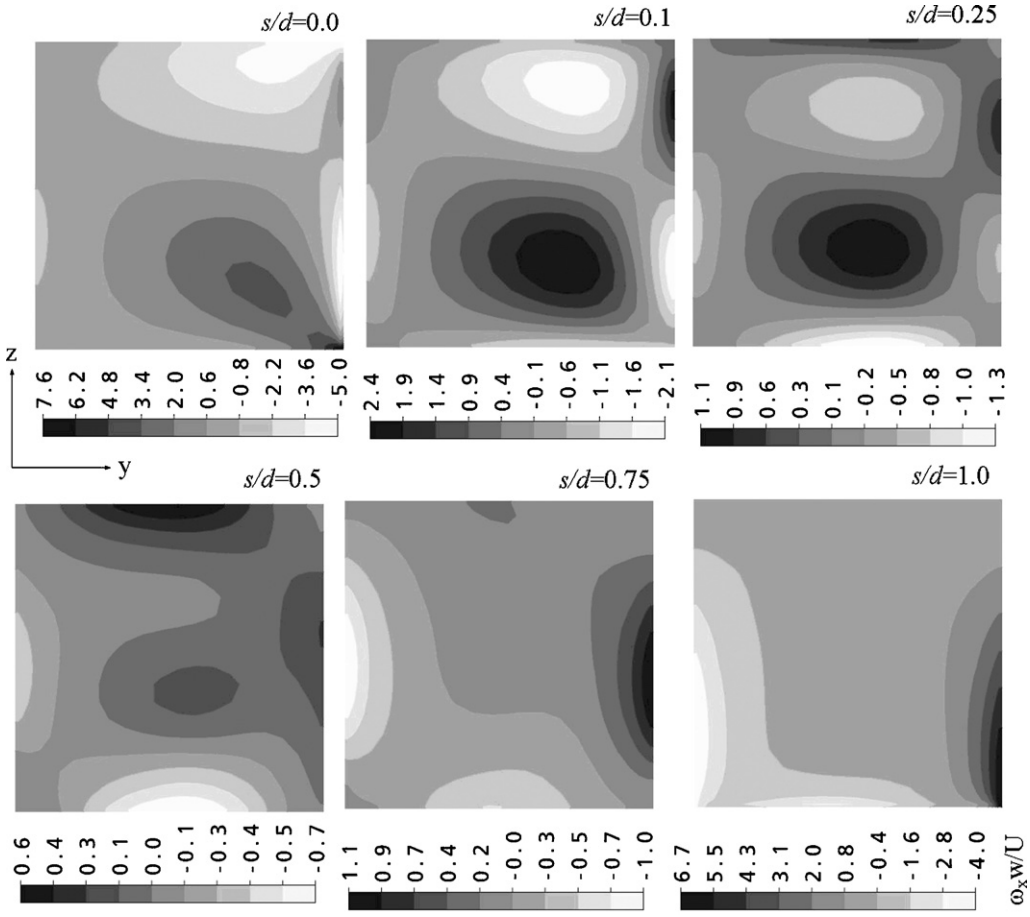

Fig. 9. Development of vorticity contours on *yz*-planes in channel-d (third L-shape unit, $Re = 10$, $h/w = 1.0$, and $d/w = 1.5$).

slightly higher than this constant value. However, this is only noted in regions limited to short distance.

Fig. 12 shows mixing index distributions in channel-d at $Re = 1$, 10, 35, and 70 for $h/w = 1.0$ and $d/w = 1.5$. As the Reynolds number increases, the level of the mixing index increases throughout most of the channel. The same trend is also seen in Fig. 10 for the circulation. The mixing index in the major portion of channel-d is almost constant. However, near the inlet and the exit, some variation of the mixing index is found. As Reynolds number increases, the variation in these regions becomes more visible. This is related to the higher circulation values (Fig. 10) and also to the larger transverse flow (Fig. 7) in the same regions.

Therefore, the aforementioned complexities in the flow are likely to enhance mixing of the fluids in those sections of the channel. However, the dominance of viscous forces at low Reynolds

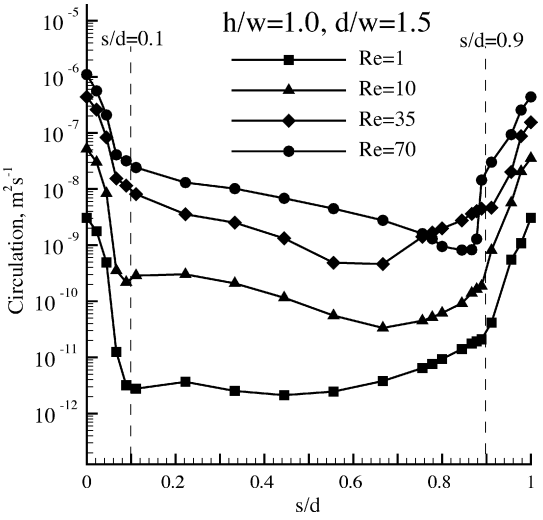

Fig. 10. Normalized circulation distributions along channel-d of third L-shape unit.

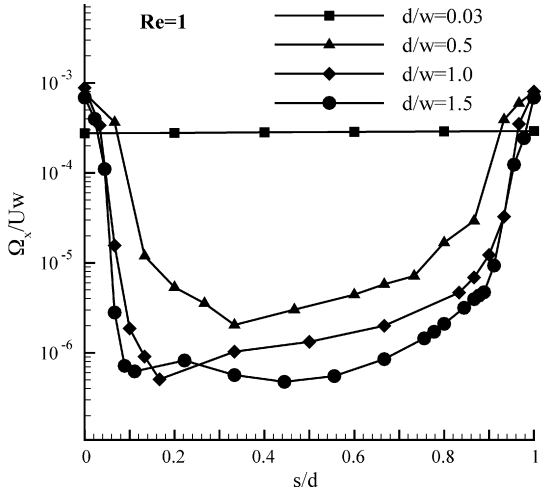

Fig. 11. Effects of d/w on circulation distribution along channel-d (third L-shape unit and $Re = 1$).

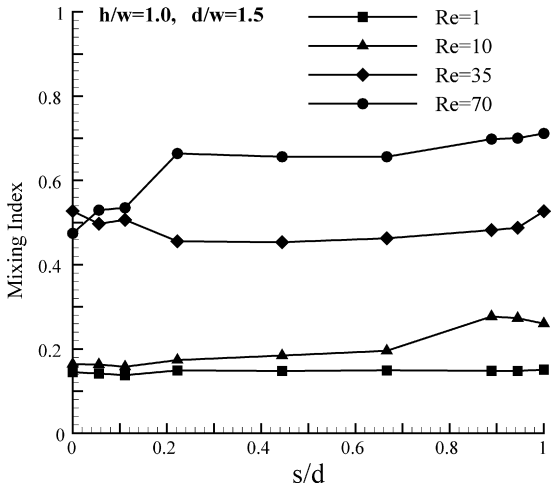

Fig. 12. Effects of Reynolds number on mixing index distribution along channel-d of third L-shape unit.

number flows in the microchannels decreases the intensity of the complex flow as the fluid passes through any straight section of the channel.

The effects of the ratio of channel height to channel width, h/w, on the mixing index for various Reynolds numbers are presented in Fig. 13, which shows the mixing index along the serpentine channel for three values of h/w, 0.50, 1.0, and 1.50, as well as for four Reynolds numbers, 1, 10, 35, and 70. It is clear that $h/w = 0.5$ and 1.5 provide better mixing performance than $h/w = 1.0$ for the Reynolds numbers 35 and 70. The surface to volume ratio of the channel is lowest for $h/w = 1.0$ among the three values of h/w. The enhanced mixing performance observed for $h/w = 0.5$ and 1.5 may be due to the fact that the interface of the two fluids is likely to undergo more stretching and folding along the channel due to the higher surface to volume ratio of the channel. However, the higher mixing shown at $h/w = 0.5$ can also be due to shorter diffusion length in the channel. The mixing characteristic for different h/w is changing with Reynolds number. At lower Reynolds numbers, $Re = 1$ and 10, the effect of h/w on mixing is low, as indicated by the close proximity of the curves for the mixing index to each other. The effect of the h/w ratio on mixing is more pronounced at higher Reynolds numbers. The mixing index distribution along x-axis for straight channel at $Re = 1$ and $h/w = 0.5$ is also shown in Fig. 13(a). The mixing index increases smoothly and slowly along x-axis. This is due to the fact that mixing is taking place only due to diffusion across the interface of the two fluids, as there is no any transverse flow like three-dimensional serpentine channel. The same trend of mixing is likely to be shown for any value of h/w ratio as in all cases the interface will be at the center of the straight microchannel. The increase in Reynolds number in straight channel will only reduce the residence time of the fluids and hence is not likely to contribute to mixing. The mixing in straight smooth channel shows same trend as reported by Stroock et al. [13].

The mixing index curves discussed in Fig. 13 shows the presence of oscillations along channel length. This can be explained with reference to Fig. 14 which shows mass fraction distribution of ethanol on xy-plane drawn at the middle of "L-shaped" unit for three dif-

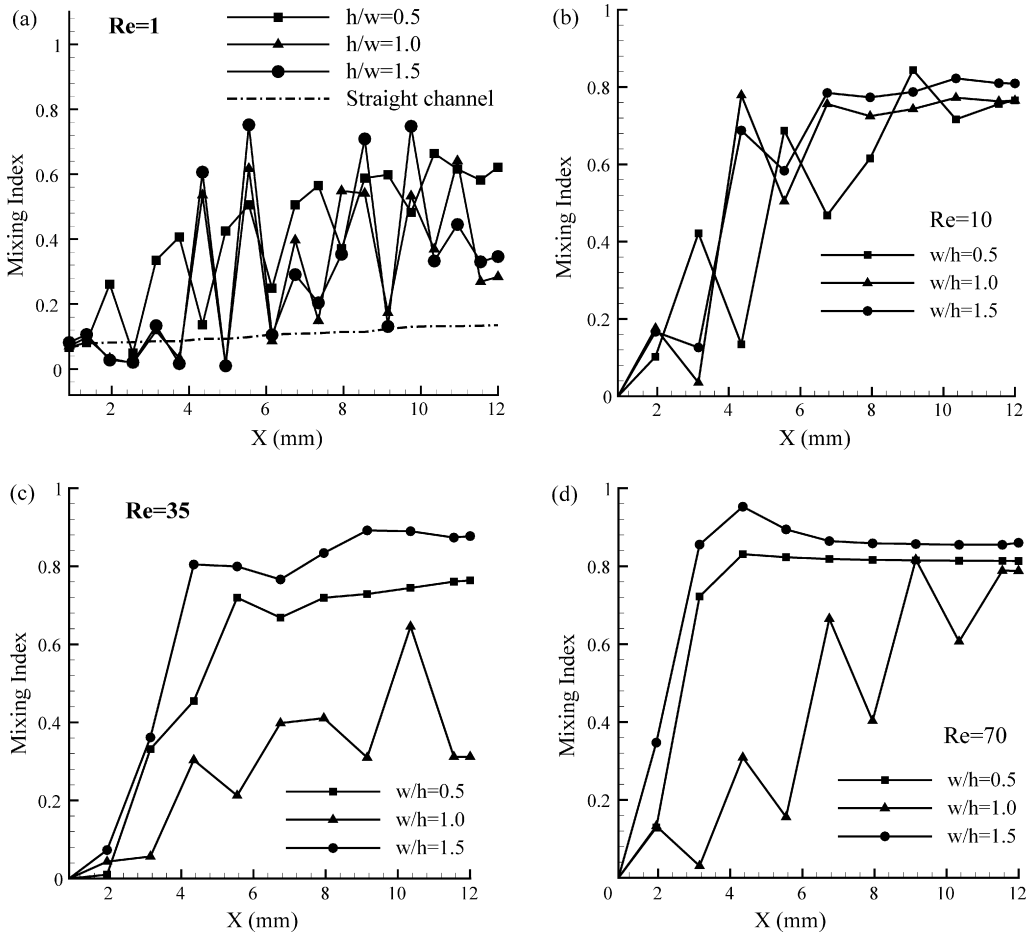

Fig. 13. Effects of h/w on mixing at $d/w = 1.0$; (a) $Re = 1$, (b) $Re = 10$, (c) $Re = 35$, and (d) $Re = 70$.

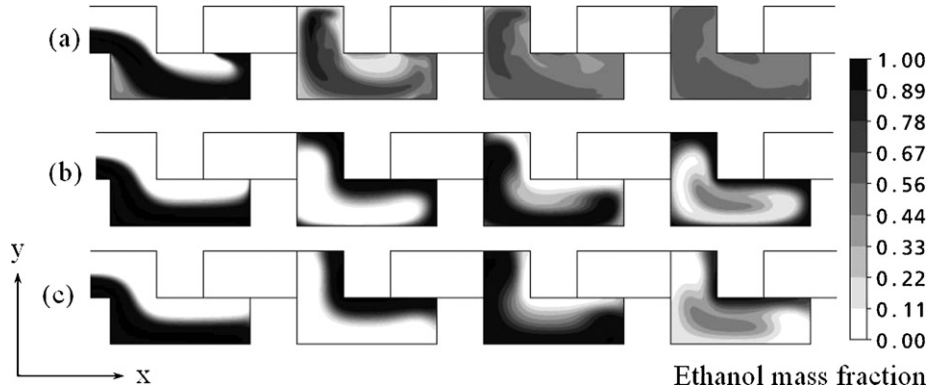

Fig. 14. Mass fraction distribution of ethanol on *xy*-plane for $d/w = 1.0$, (a) $h/w = 0.5$, $z = 0.075$ mm, $Re = 70$ (b) $h/w = 1.0$, $z = 0.15$ mm, $Re = 70$ and (c) $h/w = 1.0$, $z = 0.15$ mm, $Re = 1$.

ferent conditions. Fig. 14(a) and (b) shows the effect of h/w ratio on mass fraction distribution at $Re = 70$. The contour shows mass fraction in alternates "L-shaped" units, i.e. first, third and so on. The proportion of the mass fraction of ethanol shows oscillating trend in "L-shaped" units along channel for $h/w = 1.0$ (Fig. 14(b)) while it is relatively uniform for $h/w = 0.5$ (Fig. 14(a)). The proportion of the two fluids, ethanol and water in first "L-shaped" unit is almost same while in third unit ethanol seems more. The oscillating trend in mass fraction distribution is also depicted at $Re = 1$ for $h/w = 1$ as shown in Fig. 14(c). This is due to the reason that as the fluids flow through the three-dimensional serpentine channel it undergoes many turns on every bend. At the bend, the effect of centrifugal force may change the proportion of two fluids. And, this effect increases as h/w increases. This might be the cause for the varying proportion of mass fraction in "L-shaped" units along channel, and hence shows oscillating curve for mixing index.

Pressure drop characteristics in the serpentine channel have been analyzed, as this information is important in designing the pump needed to drive the flow in this microdevice. Fig. 15(a) and (b) shows the pressure drop characteristics of the three-dimensional serpentine microchannel for the design parameters d/w and h/w, respectively, for a channel length of 11 mm with "L-shape" repeating units for $Re = 10$. It is clear that for a fixed value of h/w, the pressure drop gradually decreases with an increase in the value of d/w for $h/w = 0.5$ 1.0, and 1.5. The rate of decrease of the pressure drop is almost the same for the three h/w ratios. The pressure drop is remarkably higher for $h/w = 0.5$ as compared to $h/w = 1.0$ or 1.5. For a given value of d/w, the pressure drop also decreases with an increase in the h/w ratio (Fig. 15(b)). For $Re = 1$ and 10, the pressure drop is not significantly affected by change to the h/w ratio. However, the effect becomes pronounced at higher Reynolds numbers, i.e., 35 and 70. The pressure drop reaches the highest value at the lowest value of h/w and the highest Reynolds number.

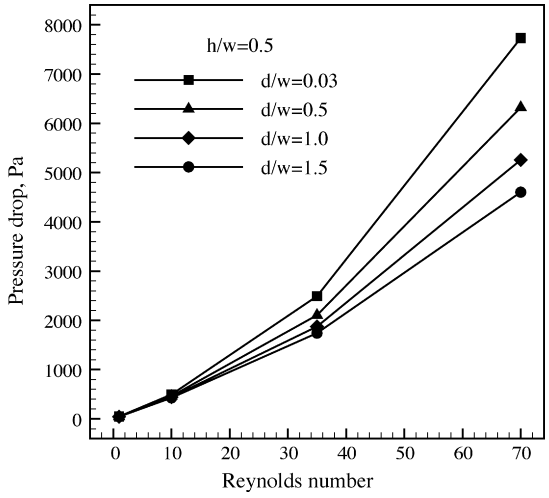

Fig. 16. Pressure drop vs. Reynolds number at $h/w = 0.5$.

Fig. 16 shows pressure drop characteristics as a function of Reynolds number for $h/w = 0.5$ and the values of d/w from 0.03 to

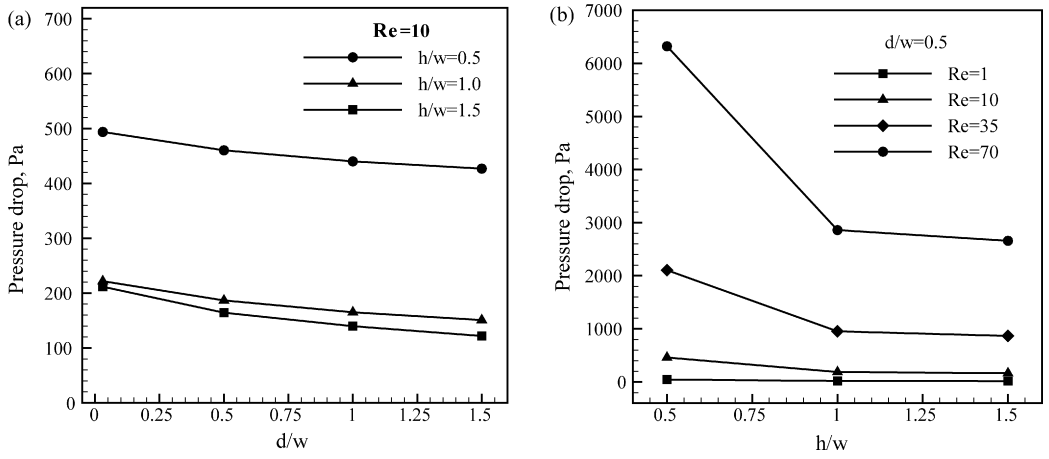

Fig. 15. Effects of geometrical parameters and Reynolds number on pressure drop; (a) d/w at $Re = 10$, and (b) h/w at $d/w = 0.5$.

1.5. The pressure drop increases with an increase in the Reynolds number for all values of d/w. At lower Reynolds numbers, i.e., $Re = 1$ and 10, the effect of d/w on the pressure drop is almost negligible. However, at higher Reynolds numbers, the pressure drop increases with a decrease in the value of d/w. The pressure drop is the highest at the lowest value of d/w, i.e. 0.03, and at the highest Reynolds number, $Re = 70$. This means that an increase in the number of bends for a given length increases the pressure loss. Hence, it is clear from the above discussion that for lower Reynolds numbers, i.e., $Re = 1$ and 10, increasing the number of bends by decreasing d/w for a given length does not increase the pressure drop.

The present analysis has been carried out with water and ethanol as working fluids with the aim to know the effect of design parameters on mixing and fluid flow. In any microchannel, mixing is affected mainly by the diffusivities of the fluids. Fluids with low diffusivities will take longer time to mix. This is likely to be true for any shape of the microchannel. However, in serpentine channel, fluids with large difference in density will also give some different behaviors due to difference in the inertia force as it passes through a series of the bends in the serpentine channel. But, it is expected that the change in working fluids does not affect significantly the effects of the geometric parameters on mixing.

4. Conclusions

A parametric study on the performance of a three-dimensional serpentine channel with "L-shaped" repeating units has been performed using computational fluid dynamics. Mixing and pressure drop characteristics have been investigated in terms of two geometric parameters i.e., the ratio of channel height to channel width, h/w, and the ratio of the length of straight channel in a "L-shaped" unit to channel width, d/w, as well as Reynolds number. The presence of bends at the end of the straight section of the "L-shaped" unit strongly influences the transverse flow structure in the channel, the vorticity contours on the planes perpendicular to the flow direction, and variation of circulation and mixing index along this region. As the Reynolds number increases from 1 to 70, both the levels of circulation and the mixing index increase throughout most of the channel. The results reveal that mixing is significantly dependent on both geometrical parameters. The mixing performance of the channel is generally improved with a decrease in the value of d/w. The mixing index shows a minimum value at $h/w = 1.0$ at higher Reynolds numbers, i.e., 35 and 70, as the lowest surface to volume ratio of the channel is found under these conditions, while the effects of h/w become negligible at lower Reynolds numbers, i.e., 1 and 10. The pressure drop characteristic of the serpentine channel is also sensitive to the two parameters. At lower Reynolds numbers, variation of the two geometrical parameters has negligible effects on the pressure drop. However, the effects of the two parameters on pressure drop become pronounced at higher Reynolds numbers. For a given Reynolds number, the pressure drop increases as both parameters, d/w and h/w, are decreased.

Acknowledgments

This work was supported by grant No. R01-2006-000-10039-0 from the Basic Research Program of the Korea Science & Engineering Foundation and the 2005 Foreign Student Researcher Invitation Program of the Korea Research Foundation.

References

[1] N.T. Nguyen, Z.G. Wu, Micromixers–review, J. Micromech. Microeng. 15 (2) (2005) R1–R16.
[2] V. Hessel, H. Lowe, F. Schonfeld, Micromixers—a review on passive and active mixing principles, Chem. Eng. Sci. 60 (8–9) (2005) 2479–2501.
[3] R.H. Liu, M.A. Stremler, K.V. Sharp, M.G. Olsen, J.G. Santiago, R.J. Adrian, H. Aref, D.J. Beebe, Passive mixing in a three-dimensional serpentine microchannel, J. Microelectromech. Syst. 9 (2) (2000) 190–197.
[4] D.J. Beebe, R.J. Adrian, M.G. Olsen, M.A. Stremler, H. Aref, B.H. Jo, Passive mixing in microchannels: fabrication and flow experiments, Mec. Ind. 2 (2001) 343–348.
[5] K.W. Lin, J.T. Yang, Chaotic mixing of fluids in a planar serpentine channel, Int. J. Heat Mass Transf. 50 (2007) 1269–1277.
[6] J.T. Yang, K.W. Lin, Mixing and separation of two-fluid flow in a micro planar serpentine channel, J. Micromech. Microeng. 16 (2006) 2439–2448.
[7] Y.Z. Liu, B.J. Kim, H.J. Sung, Two fluid mixing in a microchannel, Int. J. Heat Fluid Flow 25 (2004) 986–995.
[8] T.G. Kang, M.A. Hulsen, P.D. Anderson, J.M.J.D. Toonder, H.E.H. Meijer, Chaotic advection using passive and externally actuated particles in a serpentine channel flow, Chem. Eng. Sci. 62 (2007) 6677–6686.
[9] K.S. Lee, C. Kim, K.S. Shin, J.W. Lee, B.K. Ju, T.S. Kim, S.K. Lee, J.Y. Kang, Fabrication of round channels using the surface tension of PDMS and its application to a 3D serpentine mixer, J. Micromech. Microeng. 17 (2007) 1533–1541.
[10] C.K. Chen, C.C. Cho, Electrokinetically driven flow mixing in microchannels with wavy surface, J. Colloid Interface Sci. 312 (2007) 470–480.
[11] CFX-10.0, Solver Theory, ANSYS, 2004.
[12] S. Hardt, F. Schonfeld, Laminar mixing in different interdigital micromixers. II. Numerical simulations, AICHE J. 49 (3) (2003) 578–584.
[13] A.D. Stroock, S.K. Dertinger, A. Ajdari, I. Mezic, H.A. Stone, G.M. Whitesides, Chaotic mixer for microchannels, Science 295 (2002) 647–651.